Journal of
Applied Crystallography
ISSN 0021-8898

Received 16 August 2006
Accepted 8 January 2007

Synchrotron X-ray scattering studies on the structural evolution of microbial poly(3-hydroxybutyrate)

Kyuyoung Heo,[a] Jinhwan Yoon,[a] Kyeong Sik Jin,[a] Sangwoo Jin,[a] Gahee Kim,[a] Harumi Sato,[b] Yukihiro Ozaki,[b]* Michael M. Satkowski,[c] Isao Noda[c] and Moonhor Ree[a]*

[a]Department of Chemistry, National Research Laboratory for Polymer Synthesis and Physics, Pohang Accelerator Laboratory, Center for Integrated Molecular Systems, Polymer Research Institute, and BK School of Molecular Science, Pohang University of Science and Technology, Pohang 790-784, Republic of Korea, [b]Department of Chemistry, School of Science and Technology, Research Center for Environment Friendly Polymers, Kwansei-Gakuin University, Sanda, Hyogo 669-1337, Japan, and [c]The Procter and Gamble Company, 8611 Beckett Road, West Chester, Ohio 45069, USA. Correspondence e-mail: ozaki@kwansei.ac.jp, ree@postech.edu

The crystallization behavior of microbially synthesized poly(3-hydroxybutyrate) was studied in detail using time-resolved small-angle X-ray scattering. This polyester was found to undergo primary crystallization as well as secondary crystallization. In the primary crystallization, the thicknesses of the lamellar crystals were sensitive to the crystallization temperature, but no thickening was observed throughout the entire crystallization at a given temperature. The thickness of the lamellar crystals in the polyester was always larger than that of the amorphous layers. Secondary crystallization favorably occurred during the later stage of isothermal crystallization in competition with the continuous primary crystallization, forming secondary crystals in amorphous regions, in particular in the amorphous layers between the primarily formed lamellar crystal stacks. Compared to the primarily formed lamellar crystals, the secondary crystals had short-range-ordered structures of smaller size, a broader size distribution, and a lower electron density.

1. Introduction

Microbially synthesized, environmentally friendly poly(hydroxyalkanoate)s have attracted much attention due to their biodegradability and biocompatibility (Anderson & Dawes, 1990; Holland *et al.*, 1987; Sudesh *et al.*, 2000). A representative poly(hydroxyalkanoate) is poly(3-hydroxybutyrate) (PHB) (Fig. 1). In general, the properties of a polymer are highly dependent on its morphological structure, which in turn results from its processing conditions including crystallization. Hence, the crystallization behavior of PHB was studied by using various techniques, including differential scanning calorimetry (DSC), small- and wide-angle X-ray scattering (SAXS and WAXS), and infrared (IR) spectroscopy (Abe *et al.*, 1998; Capitan *et al.*, 2004; Chiu *et al.*, 1999; Doi *et al.*, 1995; Feng *et al.*, 2002; Gunaratne *et al.*, 2004; Kamiya *et al.*, 1991; Numata *et al.*, 2004; Pearce & Marchessault, 1994; Sato *et al.*, 2006; Sato, Murakami *et al.*, 2004; Sato, Nakamura *et al.*, 2004; Zhang *et al.*, 2005; Scandola *et al.*, 1992). In particular, the SAXS technique has been employed to investigate the morphological structure of PHB already crystallized from the melt (Abe *et al.*, 1998; Capitan *et al.*, 2004; Chiu *et al.*, 1999; Numata *et al.*, 2004). Recent IR spectroscopy studies found that in the lamellar crystals of PHB, there is hydrogen bonding between the methyl group of one helical structure and the carbonyl group of another helical structure along an axis of the crystal lattice, and such hydrogen bonding stabilizes the chain folding in the lamellar crystals (Sato *et al.*, 2006; Sato, Murakami *et al.*, 2004; Sato, Nakamura *et al.*, 2004; Zhang *et al.*, 2005). However, detailed studies on the evolution of morphological structures in this microbial polyester and its crystallization mechanism are still needed.

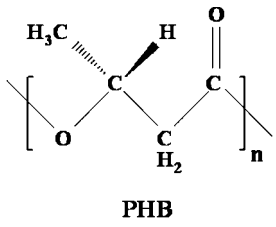

PHB

Figure 1
Chemical structure of poly(3-hydroxybutyrate) (PHB).

Therefore, to better understand the structural evolution of PHB and the resulting morphological structures, in the present work we performed detailed time-resolved SAXS studies during the isothermal crystallization of PHB polymer.

2. Experiment

A bacterially synthesized PHB polymer (4.37×10^5 weight-average molecular weight) was obtained from the Proctor and Gamble Co. The polyester was dissolved in hot chloroform, and then reprecipitated in methanol as a fine powder, followed by drying at 333 K in vacuum. Thereafter, the polymer was melt-molded under compres-

sion in a nitrogen atmosphere and cooled to room temperature, giving 2 mm thick sheets. These polymer sheets were cut into discs with a diameter of 4 mm for use in SAXS measurements. SAXS measurements were carried out at the 4C1 SAXS beamline of the Pohang Accelerator Laboratory (Bolze *et al.*, 2002; Lee *et al.*, 2002, 2003, 2004; Ree & Ko, 2005; Yu *et al.*, 2005). The wavelength λ of the X-ray beam was 1.608 Å; the X-ray beam size at the sample stage was 1×1 mm. A two-dimensional (2D) charge-coupled detector (CCD) (Mar USA, Inc.) was employed. The distance between sample and detector was 1.0 m. SAXS measurements were carried out during isothermal crystallization of the polymer samples over 398–418 K. Each measurement was collected for 20 s. In the measurements, a jumping hot stage consisting of two independent chambers under a nitrogen atmosphere was employed to conduct isothermal experiments, and the temperatures of the chambers as well as the polymer sample were individually controlled and monitored by Eurotherm controllers with a K-type thermocouple. Each sample was first melted for 5 min in the top chamber and then quickly jumped to the bottom chamber, which was held at the chosen crystallization temperature T_c. Each 2D SAXS data set was circular averaged from the beam center, and then normalized to the incident X-ray beam intensity, which was monitored by an ionization chamber placed in front of the sample and corrected further for the background run. DSC thermograms were measured using a Seiko calorimeter calibrated with indium and tin standards. In the DSC measurements, all polymer samples were first melted for 5 min and then jumped to the chosen crystallization temperature T_c, at which they underwent isothermal crystallization, as described above for SAXS measurements, and then remelted at a heating rate of 3.0 K min^{-1}. The DSC measurements were further conducted at a heating rate of 10.0 K min^{-1} for the samples cooled to 203 K from the melt. It was found that the glass transition temperature T_g of the PHB polymer was 269 K. All the DSC measurements were also carried out under a nitrogen atmosphere.

3. Results and discussion

Fig. 2 shows typical time-resolved SAXS patterns measured for PHB polymer undergoing isothermal crystallization at 418 K. As can be seen from the figure, the SAXS pattern is not detected initially but develops with the structural evolution associated with crystallization. With crystallization time the SAXS peak increases in intensity, and its peak maximum shifts to the high q region, finally remaining unchanged with further increase in the crystallization time. Similar SAXS patterns with crystallization time were observed for the polymer undergoing isothermal crystallization at other crystallization temperatures (data not shown).

The measured SAXS profiles $I(q)$ were nonlinear-least-squares fitted with Porod's law (Koberstein & Stein, 1983; Lee *et al.*, 2003; Ruland, 1971):

$$\lim_{q\to\infty} I(q) = I_b + (K_p/q^4)\exp(-\sigma^2 q^2), \qquad (1)$$

where $I(q)$ is the scattering intensity profile, I_b is the constant scattering from density fluctuations, σ is related to the interfacial thickness between the lamellar crystal and the amorphous layer, K_p is the Porod constant, and q is given by $q = (4\pi/\lambda)\sin\theta$, where λ is the wavelength of the X-ray source and 2θ is the scattering angle.

For the measured SAXS data, the Porod region was found to start around $q = 1.48$ nm^{-1}. Taking this fact into account, Porod fitting of the measured SAXS profile was performed over the range of $1.48 \leq q \leq 2.89$ nm^{-1}. In this fitting, we considered σ as a variable, and then found that σ ranges from 0.1 to 1.1 nm depending on the crystallization temperature and time. During the isothermal crystallizations, the σ value was very small at the initial stage of isothermal crystallization but increased rapidly with increasing time and then turned to show slow increases with further increasing time; the σ value was relatively larger for the sample crystallized at a higher temperature. Overall, these σ values are much smaller than the lamellar crystal thicknesses determined in our study. Furthermore, it is noted that in our study morphological parameters (*i.e.*, long period L, lamellar crystal thickness d_c, and amorphous layer thickness d_a) determined from the SAXS profile calculated with the contribution of σ are very close to those determined from the SAXS profile calculated without the contribution of σ. Taking these results into account, we attempted to extrapolate the fitted SAXS profile to $q > 2.89$ nm^{-1} to determine the I_b term, and then found that I_b is the same for the extrapolations to $q \geq 5.0$ nm^{-1}. Thus, I_b was determined, after which the fitted SAXS profile was extrapolated to $q = 5$ nm^{-1}. The I_b values were subtracted from the SAXS profile, which was then corrected by multiplying by q^2, giving the Lorentz-corrected SAXS profile.

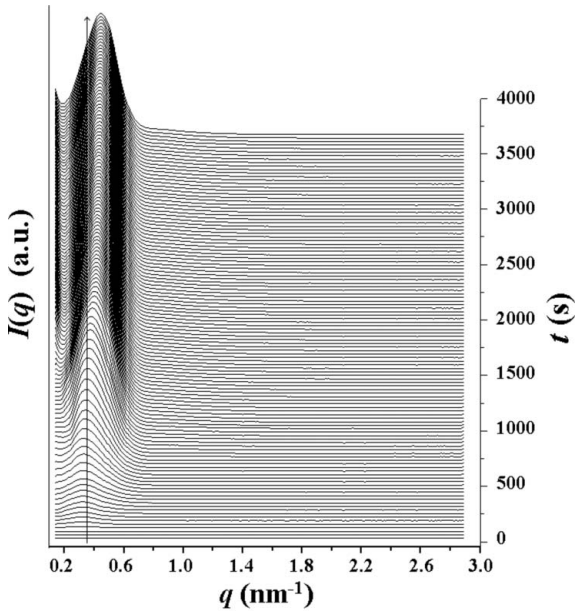

Figure 2
Time-resolved SAXS patterns of PHB polymer measured during isothermal crystallization at 418 K for 60 min.

The Lorentz-corrected SAXS profile can be analyzed by one-dimensional correlation function analysis (Goderis *et al.*, 1999; Lee *et al.*, 2002, 2003; Strobl & Schneider, 1980; Vonk & Kortleve, 1967) and/or interface distribution function analysis (Ruland, 1977; Albrecht & Strobl, 1996; Verma *et al.*, 1996; Santa Cruz *et al.*, 1991; Xia *et al.*, 2001) in order to determine the morphological parameters. Both of these approaches were considered for analyzing the SAXS data of our study. However, we found that in the interface distribution function analysis all peaks often reveal a broad nature and consequently overlap in part or heavily, depending on the sample composition as well as the crystallization temperature and time. Such broadness and overlapping of the peaks cause great difficulty in determining the peak maximum and minimum that directly correlate to the morphological parameters, leading to significant uncertainties in the determined morphological parameters. Further, our study found that the long period L determined directly from the Lorentz-corrected SAXS profile is very often mismatched with that obtained by the interface distribution function analysis but well matched with that obtained by the correlation function analysis. Therefore, in our

study we analyzed the Lorentz-corrected SAXS profiles using the one-dimensional correlation function method.

The Lorentz-corrected SAXS profile was inverse-cosine Fourier transformed to a one-dimensional correlation function $\gamma_1(z)$ in order to determine the morphological parameters (Goderis *et al.*, 1999; Lee *et al.*, 2002, 2003; Strobl & Schneider, 1980; Vonk & Kortleve, 1967):

$$\gamma_1(z) = \int_0^\infty q^2 I(q) \cos(qz)\, \mathrm{d}q, \tag{2}$$

where z is the direction normal to the layer faces in the stack. The one-layer thickness l_1 in the lamellar crystal and amorphous layer stack was determined from the linear fit of the first decay slope in the plot of $\gamma_1(z)/\gamma_1(0)$ *versus* z. The long period L was obtained from the first peak maximum (z_{max}) of the same plot, and the other layer thickness l_2 (= $L - l_1$) can be obtained from L and l_1. The invariant Q was also determined from the Lorentz-corrected SAXS profile by (Ruland, 1971; Koberstein & Stein, 1983; Vonk & Kortleve, 1967; Jonas *et al.*, 1994)

$$Q = \int_0^\infty q^2 I(q)\, \mathrm{d}q. \tag{3}$$

Fig. 3 shows representative correlation functions, which were obtained from the Lorentz-corrected SAXS profiles of the PHB polymer isothermally crystallizing at 418 K. From the correlation function analysis, the structural parameters (l_1, l_2, and L) were determined with crystallization time. The results are presented in Fig. 4.

As can be seen in Figs. 3 and 4, as the crystallization time increases at a chosen crystallization temperature, l_1 and L decrease while l_2 varies very little. Furthermore, l_1 is always shorter than l_2 (= $L - l_1$) regardless of the crystallization temperature and time. Here l_1 can be assigned to either the lamellar crystal thickness or the amorphous layer thickness of the lamellar stacks formed in the polymer samples, according to Babinet's reciprocity. Thus, to assign l_1 we need additional experimental evidence.

DSC measurements were conducted for the PHB samples crystallized isothermally for 3600 s at 398, 408, and 418 K. The crystal melting temperature was determined to be 443.9 K for the sample crystallized at 398 K, 445.7 K for the sample crystallized at 408 K, and 447.2 K for the sample crystallized at 418 K. For the samples crystallized under the same conditions as in the DSC measurements, the SAXS analysis found that as the crystallization temperature increased from 398 to 418 K, l_1 ranged from 2.76 to 3.75 nm while l_2 ranged from 5.79 to 8.87 nm. With increasing crystallization temperature the increases in the l_1 values are relatively much smaller than those in the l_2 values. In general, lamellar crystals of larger thickness in crystalline polymers reveal higher melting temperature (Goderis *et al.*, 1999; Lee *et al.*, 2002, 2003, 2004; Strobl & Schneider, 1980; Vonk & Kortleve, 1967; Ruland, 1971; Koberstein & Stein, 1983; Vonk & Kortleve, 1967). Taking into account this fact together with the observation that l_1 is always shorter than l_2, we assign l_2, which shows relatively large increases with increasing crystallization temperature, to the lamellar crystal thickness d_c. l_1, which shows relatively small increases with increasing crystallization temperature, is assigned to the amorphous layer thickness d_a.

Taking these d_c and d_a assignments into account, the SAXS measurements and data analysis provide important information on the isothermal crystallization and resulting morphology of PHB as follows. First, the thickness d_c of the lamellar crystals (primary crystals) is dependent on the crystallization temperature for all the polymers (Fig. 4), indicating that the degree of supercooling is the major driving force in determining the lamellar crystal thickness.

Second, d_c varies very little during the entire crystallization process, even including the later stages of crystallization (Fig. 4). These results indicate that the primarily formed crystals are not thickened through the whole isothermal crystallization process. In the crystallization of these polymers, secondary crystallization was observed to occur in addition to the primary crystallization; the secondary crystallization will be discussed in detail later. Taking this fact into account, the formation of the secondary crystals contributes very little to d_c. These results indicate that the secondary crystals are formed with a very low density with respect to that of the primarily formed lamellar crystals; namely the density of the secondary crystals is too low to reflect in the d_c values determined by the SAXS analysis, which result mainly from the primary lamellar crystals.

Third, the amorphous layer thickness d_a decreases during the primary crystallization (Fig. 4), which is quite different from the

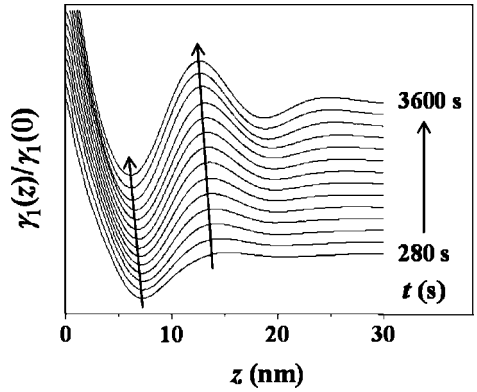

Figure 3
Correlation function $\gamma_1(z)/\gamma_1(0)$ obtained from the Lorentz-corrected SAXS intensity profiles, which were measured during the isothermal crystallization of PHB at 418 K for 60 min.

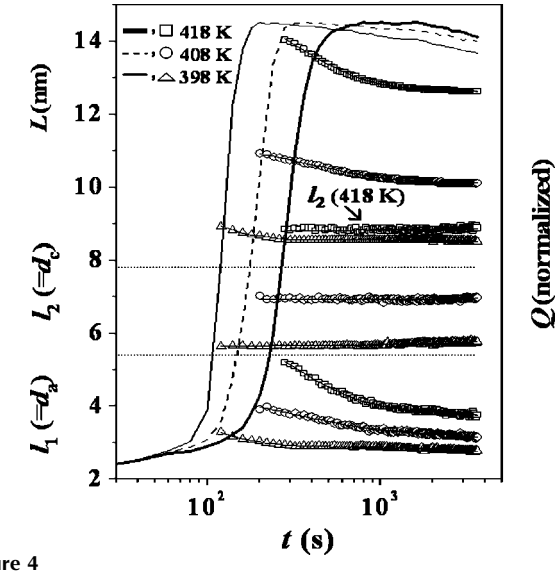

Figure 4
Variations of morphological parameters (long period L, lamellar crystal thickness d_c and amorphous layer thickness d_a) with time obtained from the SAXS patterns measured during isothermal crystallization of PHB at various temperatures. The time dependence of the invariant Q obtained from the SAXS patterns measured during the isothermal crystallizations is plotted together with the determined morphological parameters; here, the variation of Q with time at each crystallization temperature was normalized by its maximum value. The symbols represent the noted morphological parameters; the solid lines indicate the values of the invariant Q.

behavior of the lamellar crystal thickness d_c. Various factors could potentially contribute to the observed decrease in d_a during the primary crystallization, including the distribution of d_a in the lamellar stacks and its variation with time, the number of lamellae in the lamellar stacks and its effect on the SAXS profile, and relaxation of the polymer chains in the amorphous layers.

Fourth, the amorphous layer thickness d_a further decreases during the later stage of the crystallization process (*i.e.*, the secondary crystallization process) (Fig. 4). However, the changes in d_a as a result of the secondary crystallization are less than 8% of the amorphous layer thickness in the lamellar crystal stack formed during the primary crystallization, which might be due to low population and limited growth and perfectioning of secondary crystals. These results suggest that the secondary crystals are formed in the amorphous layers in the lamellar stacks formed during the primary crystallization and in the amorphous regions between the lamellar stacks.

Finally, the long period L decreases during the entire crystallization (Figs. 2–4) and shows a similar trend to that observed in the variation of amorphous layer thickness d_a. The decrease in L is less than 17% of the value of L in the lamellar stacks formed during the primary crystallization (Fig. 4).

In addition, the change in the invariant Q with the crystallization time was determined from the SAXS patterns measured during the isothermal crystallization. As can be seen in Fig. 4, the value of Q is small and constant for an initial induction period, then increases rapidly with time, reaches a maximum, and then decreases slowly.

In general, the invariant Q of a crystalline polymer is proportional to the product of several structural parameters: the volume fraction of lamellar stacks (α_s) within the total irradiated sample volume, the volume fraction of the crystalline and amorphous phases in the lamellar stacks [φ_c and φ_a ($= 1 - \varphi_c$)] and the squared product of the difference between the temperature-dependent electron densities of the crystalline and amorphous phases (ρ_c and ρ_a) (Goderis *et al.*, 1999; Lee *et al.*, 2002, 2003; Strobl & Schneider, 1980; Vonk & Kortleve, 1967; Ruland, 1971; Koberstein & Stein, 1983). Taking these parameters into account, during the primary crystallization the invariant Q always increases rapidly due to contributions of all the structural parameter terms developed with the crystallization time. This trend is evident in all the measured values of the invariant Q (Fig. 4). On the other hand, for the later stage of crystallization (*i.e.*, secondary crystallization), the parameter α_s may vary very little but could not decrease with time. The term $\varphi_c\varphi_a$ [$= \varphi_c(1 - \varphi_c)$] may vary with time, contributing to a variation in the invariant Q. However, the φ_c term generally increases slightly with time during the secondary crystallization. Because of this, the contribution of the $\varphi_c\varphi_a$ term to the invariant Q is relatively small. In comparison, the term $(\rho_c - \rho_a)^2$ ($= \Delta\rho^2$) contributes significantly to the variation in the invariant Q. Taking these facts into account, the observation that Q decreases slowly with time during the secondary crystallization results from a reduction in the $\Delta\rho$ term with time. As the value of ρ_c would not decrease with the crystallization time, the decrease in the $\Delta\rho$ term is attributed to the increase in ρ_a, signifying a densification of the amorphous layers *via* the secondary crystallization. This densification shrinks the amorphous layers, consequently reducing the amorphous layer thickness d_a. This reduction of d_a is evident in the present study (Fig. 4) as already discussed above.

Collectively, these time-resolved SAXS measurements and data analysis found that the PHB polymer undergoes favorably primary crystallization, producing lamellar crystal stacks and volume-filling the sample specimen with the lamellar crystal stacks before the commencement of secondary crystallization, and thereafter forms secondary crystals in the amorphous layers in the lamellar stacks formed during the primary crystallization and in the amorphous regions between the lamellar stacks. The secondary crystals formed in the amorphous regions characteristically have an electron density much lower than that of the primarily formed lamellar crystals.

4. Conclusions

We determined the morphological parameters (*i.e.*, long period, lamellar crystal thickness, and amorphous layer thickness) as a function of time and temperature during the isothermal crystallization of the microbial PHB polymer. The polyester was found to undergo primary and secondary crystallization. The primary crystals formed first, and the secondary crystals formed at a later stage of crystallization in competition with the continuous primary crystallization. This secondary crystallization occurred in the amorphous regions, in particular in the amorphous layers between the primarily formed lamellar crystal stacks. Compared to the primary lamellar crystals, the secondary crystals were characterized by a short-range-ordered structure of smaller size and a lower electron density. The PHB polymer formed primary lamellar crystal stacks that were thicker than the amorphous layers.

This work was supported by the Korea Science and Engineering Foundation (National Research Laboratory Program: Contract No. M10500000068-06J0000-6810) and by the Korean Ministry of Education (Brain Korea 21 Program). Synchrotron SAXS measurements were supported by the Ministry of Science and Technology and POSCO.

References

Abe, H., Doi, Y., Aoki, H. & Akehata, T. (1998). *Macromolecules*, **31**, 1791–1797.
Albrecht, T. & Strobl, G. (1996). *Macromolecules*, **29**, 783–785.
Anderson, A. J. & Dawes, E. A. (1990). *Microbiol. Rev.* **54**, 450–472.
Bolze, J., Kim, J., Huang, J.-Y., Rah, S., Youn, H. S., Lee, B., Shin, T. J. & Ree, M. (2002). *Macromol. Res.* **10**, 2–12.
Capitan, M. J., Rueda, D. R. & Ezquerra, T. A. (2004). *Macromolecules*, **37**, 5653–5659.
Chiu, H.-J., Chen, H.-J., Lin, T.-L. & Lin, J. S. (1999). *Macromolecules*, **32**, 4969–4974.
Doi, Y. (1990). *Microbial Polyester*. New York: VCH Publishers Inc.
Doi, Y., Kitamura, S. & Abe, H. (1995). *Macromolecules*, **28**, 4822–4828.
Feng, L., Watanabe, T., Wang, Y., Kichize, T., Fukuchi, T., Chen, G.-Q., Doi, Y. & Inoue, Y. (2002). *Biomacromolecules*, **3**, 1071–1077.
Goderis, B., Reynaers, H., Koch, M. H. J. & Mathot, V. B. F. (1999). *J. Polym. Sci. Polym. Phys. Ed.* **37**, 1715–1738.
Gunaratne, L. M. W. K., Shanks, R. A. & Amarasinghe, G. (2004). *Thermochim. Acta*, **423**, 127–135.
Holland, S. J., Jolly, A. M., Yasin, M. & Tighe, B. J. (1987). *Biomaterials*, **8**, 289–295.
Jonas, A. M., Russell, T. P. & Yoon, D. Y. (1994). *Colloid Polym. Sci.* **272**, 1344–1351.
Kamiya, N., Sakurai, M., Inoue, Y., Chujo, R. & Doi, Y. (1991). *Macromolecules*, **24**, 2178–2182.
Koberstein, J. T. & Stein, R. S. (1983). *J. Polym. Sci. Polym. Phys. Ed.* **21**, 2181–2200.
Lee, B., Shin, T. J., Lee, J. W. & Ree, M. (2002). *Macromol. Symp.* **190**, 173–184.
Lee, B., Shin, T. J., Lee, S. W., Yoon, J. & Ree, M. (2004). *Macromolecules*, **37**, 4174–4184.
Lee, B., Shin, T. J., Lee, S. W., Yoon, J., Youn, H. S., Lee, K.-B. & Ree, M. (2003). *Polymer*, **44**, 2509–2518.
Numata, K., Hirota, T., Kikkawa, Y., Tsuge, T., Iwata, T., Abe, H. & Doi, Y. (2004). *Biomacromolecules*, **5**, 2186–2194.
Pearce, R. & Marchessault, R. H. (1994). *Polymer*, **35**, 3990–3997.
Ree, M. & Ko, I. S. (2005). *Phys. High Tech.* **14**, 2–7.
Ruland, W. (1971). *J. Appl. Cryst.* **4**, 70–73.
Ruland, W. (1977). *Colloid Polym. Sci.* **255**, 417–427.

Santa Cruz, C., Stribeck, N. & Zachmann, H. G. (1991). *Macromolecules*, **24**, 5980–5990.
Sato, H., Mori, K., Murakami, R., Yuriko, A., Takahashi, I., Zhang, J., Terauchi, H., Hirose, F., Senda, K., Tashiro, K., Noda, I. & Ozaki, Y. (2006). *Macromolecules*, **39**, 1525–1531.
Sato, H., Murakami, R., Padermshoke, A., Hirose, F., Senda, K., Noda, I. & Ozaki, Y. (2004). *Macromolecules*, **37**, 7203–7231.
Sato, H., Nakamura, M., Padermshoke, A., Yamaguchi, H., Terauchi, H., Ekgasit, S., Noda, I. & Ozaki, Y. (2004). *Macromolecules*, **37**, 3763–3769.
Scandola, M., Ceccorulli, G., Pizzoli, M. & Gazzano, M. (1992). *Macromolecules*, **25**, 1405–1410.
Strobl, G. R. & Schneider, M. (1980). *J. Polym. Sci. Polym. Phys. Ed.* **18**, 1343–1359.
Sudesh, K., Abe, H. & Doi, Y. (2000). *Prog. Polym. Sci.* **25**, 1503–1555.
Verma, R., Marrand, H. & Hsiao, B. (1996). *Macromolecules*, **29**, 7767–7775.
Vonk, C. G. & Kortleve, G. (1967). *Colloid Polym. Sci.* **220**, 19–24.
Xia, Z., Sue, H.-J., Wang, Z., Avila-Orta, C. A. & Hsiao, B. S. (2001). *J. Macromol. Sci. B Phys.* **40**, 625–638.
Yu, C.-J., Kim, J., Kim, K.-W., Kim, G.-H., Lee, H.-S., Ree, M. & Kim, K.-J. (2005). *J. Korean Vac. Soc.* **14**, 138–142.
Zhang, J., Sato, H., Noda, I. & Ozaki, Y. (2005). *Macromolecules*, **38**, 4274–4281.